The Response of a Spherical Tissue-Equivalent Proportional Counter to Iron Particles from 200–1000 MeV/nucleon

B. B. Gersey,[a] T. B. Borak,[a,1] S. B. Guetersloh,[a] C. Zeitlin,[b] J. Miller,[b] L. Heilbronn,[b] T. Murakami[c] and Y. Iwata[c]

[a] Department of Radiological Health Sciences, Colorado State University, Fort Collins, Colorado 80523; [b] Life Sciences Division, Lawrence Berkeley National Laboratory, Berkeley, California 94720; and [c] Division of Accelerator Physics and Engineering, National Institute of Radiological Sciences, 9-1 Anagawa 4-chome, Inage-ku, Chiba 263, Japan

Gersey, B. B., Borak, T. B., Guetersloh, S. B., Zeitlin, C., Miller, J., Heilbronn, L., Murakami, T. and Iwata, Y. The Response of a Spherical Tissue-Equivalent Proportional Counter to Iron Particles from 200–1000 MeV/nucleon. *Radiat. Res.* 157, 350–360 (2002).

The radiation environment on board the space shuttle and the International Space Station includes high-Z and high-energy (HZE) particles that are part of the galactic cosmic radiation (GCR) spectrum. Iron-56 particles are considered to be one of the most biologically important parts of the GCR spectrum. Tissue-equivalent proportional counters (TEPCs) are used as active dosimeters on manned space flights. These TEPCs are further used to determine the average quality factor for each space mission. A TEPC simulating a 1-μm-diameter sphere of tissue was exposed as part of a particle spectrometer to ^{56}Fe particles at energies from 200–1000 MeV/ nucleon. The response of TEPCs in terms of mean lineal energy, $\bar{y}_F$, and dose mean lineal energy, $\bar{y}_D$, as well as the energy deposited at different impact parameters through the detector was determined for six different incident energies of ^{56}Fe particles in this energy range. Calculations determined that charged-particle equilibrium was achieved for each of the six experiments. Energy depositions at different impact parameters were calculated using a radial dose distribution model, and the results were compared to experimental data. © 2002 by Radiation Research Society

INTRODUCTION

It has been estimated that during a 3-year mission to Mars, an astronaut would receive a radiation dose equivalent of 1 Sv (*1*). During space travel outside of the geomagnetosphere, the main source of chronic radiation exposure is from galactic cosmic radiation (GCR). Approximately 87% of the particles in the GCR spectrum are protons, 12% are helium nuclei, and 1% are particles heavier than helium, often referred to as high-Z and high-energy (HZE) particles. The heaviest biologically important particle of these HZE particles is iron because of its relatively large contribution to radiation dose and its high LET (*1, 2*).

Currently, tissue-equivalent proportional counters (TEPCs) are flown on board the Space Shuttle and International Space Station as area monitors to characterize the radiation field inside the spacecraft (*3–5*). Energy deposition spectra produced by a TEPC can be used to calculate absorbed dose and to estimate the average quality of radiation during the mission (*6*). In these analyses, it was assumed that lineal energy, y, is numerically equivalent to LET (*7, 8*). Thus the measured distribution $f(y)$ was assumed to be a direct measurement of the LET spectrum of the incident particles. However, recent comparisons of measurements of $f(y)$ with a TEPC and $f(L)$ using a particle spectrometer indicate that there are major differences between the two distributions (*9*). This can cause large uncertainties in the corresponding estimates of quality factor. The objective of these studies was to determine the response of tissue-equivalent proportional counters similar to those used for practical dosimetry of HZE particles in the GCR spectrum. The intent was not to make precise measurements of the track structure for ^{56}Fe particles, but rather to understand how inherent track structure influences the response and the interpretation of data obtained with such detectors.

Previous measurements of the response of TEPCs have used particle accelerators to produce HZE radiation of energies similar to those found in the GCR spectrum. Table 1 summarizes some of these experiments. Glass and Braby (*10*) exposed a wall-less microdosimeter to a broad beam of α particles. In this experiment, comparisons were made between the measured energy deposition and a calculated theoretical response function. In a series of experiments by Rodgers *et al.* (*11*), both a walled and a wall-less microdosimeter simulating a 2-μm-diameter sphere of tissue were exposed to 3.9 GeV/nucleon nitrogen ions. Distributions of lineal energy were determined for both counters at various depths in a water and a plastic phantom. Measurements were made to compare the responses of the walled and wall-less detectors under identical irradiation conditions. Kliauga *et al.* (*12*) performed a series of irradiations

TABLE 1
Previous Experiments with HZE Particle Beams Using a TEPC

Reference	TEPC type	Particle species	Particle beam energy (MeV/nucleon)	Position and particle identification
Glass and Braby (*10*)	Spherical wall-less	Helium	1.125	None
Rodgers *et al.* (*11*)	Spherical walled, spherical wall-less	Nitrogen	3900	None
Kliauga *et al.* (*12*)	Spherical wall-less	Carbon, argon	400, 450	None
π				
Luxton and Fessenden (*13*)	Spherical walled	Helium, carbon, neon	230, 400, 400	None
Dicello *et al.* (*15*)	Spherical walled		167	None
Metting *et al.* (*16*)	Cylindrical wall-less	Iron	600	One-dimensional postitional and species determination by PSD
Dicello and Wasiolek (*14*)	Spherical walled, cylindrical wall-less	Iron, argon, neon, carbon	535, 570, 557, 400	None
Ito and Henkelman (*17*)	Spherical walled		180	Time-of-flight velocity determination
Rademacher *et al.* (*18*)	Spherical walled	Iron	1050	Two-dimensional positional and species determination by PSDs

exposing two wall-less microdosimeters to 400 MeV/nucleon ^{12}C and 450 MeV/nucleon ^{40}Ar particle beams. A ridge filter was used to spread out the Bragg peaks of the incident ions. Energy response spectra of the wall-less microdosimeters were taken at several points along these Bragg peaks. Luxton and Fessenden (*13*) irradiated a 12.7-mm-diameter TEPC with a 2.5-mm tissue-equivalent (TE) wall. This TEPC simulated a 2-μm-diameter sphere of tissue using a TE gas at a pressure of 67 Torr in the active chamber volume. This series of experiments found values for the dose-averaged lineal energy of carbon, helium and neon particles at initial energies of 400 MeV/nucleon, 230 MeV/nucleon and 400 MeV/nucleon, respectively. Dose-averaged lineal energy values were also taken for these three particle beams as each beam was modified with a variable-thickness water column. Dicello *et al.* (*14*) compared measurements of microdosimetric spectra for energetic ion beams using a spherical walled detector and a cylindrical wall-less detector. They observed a large range of energy depositions including very large events. All of the above experiments observed differences between walled and wall-less detectors, but they could only speculate about the reasons for the shapes of the distributions or make qualitative comparisons with theory because they did not have precise information on the type (i.e. incident ion or fragment) or location of the particles as they entered the detector. They did not discuss how many of the observed differences were due to δ rays associated with track structure, beam inhomogeneity, and artifacts relating to the design of the detector.

Metting *et al.* (*16*) determined energy deposition in a wall-less microdosimeter as a function of impact parameter for 600 MeV/nucleon ^{56}Fe particles. They were able to measure energy deposition as a function of radial distance from the track. This provided information concerning the dimensions of the track as well as characteristics of energy deposition as a function of radius. Ito and Henkelmen (*17*) irradiated a 12.7-mm-diameter microdosimeter simulating a 2-μm-diameter sphere of tissue in a negative pion beam. They used time-of-flight techniques to differentiate between particles that had the same momentum but different velocities. This enabled them to resolve the microdosimetric spectra into contributions from pions, muons and electrons. They did not have information on differences in spatial characteristics for each component of the beam. An experiment performed by Rademacher *et al.* (*18*) used a solid-walled 12.7-mm-diameter TEPC that was exposed to 1.05 GeV/nucleon ^{56}Fe particles. The detector was part of a particle spectrometer consisting of thin silicon detectors that could identify both the type and position of the incident particles upstream and downstream of the TEPC. They measured the patterns of energy deposition as a function of trajectory through the detector and made a quantitative assessment of how the wall affects this response.

In the present series of experiments, data were obtained at particle accelerator facilities that produced beams of ^{56}Fe particles with kinetic energies between 200 and 1000 MeV/nucleon (β = v/c = 0.56–0.88). Specifically, a spherical TEPC was exposed to ^{56}Fe-particle beams at energies spanning the peak of the GCR iron-particle spectrum. In each case, a particle spectrometer measured the charge and position of each incident particle both upstream and downstream of the TEPC. With this experimental arrangement, the type of incident particle as well as the trajectory of the particle through the TEPC could be reconstructed and related to the energy deposition recorded by the detector. Frequency distributions of energy deposition (i.e. response functions) were determined for uniformly incident beams of ^{56}Fe particles, and these distributions were used to com-

Experiment name	Extracted beam energy (MeV/nucleon)	Energy at entrance to TEPC gas cavity (MeV/nucleon)	Velocity of ^{56}Fe(β)	Maximum energy of electron ejected from ^{56}Fe-particle track (MeV)
HIMAC00	250	200	0.57	0.48
HIMAC99	400	360	0.69	0.93
BNL97_1	600	540	0.77	1.51
BNL98	1087	700	0.82	2.09
BNL97_2	1087	790	0.84	2.44
BNL99	1087	1000	0.87	3.33

pute absorbed dose as well as average values of lineal energy, y.

MATERIALS AND METHODS

Six experiments were performed, four with the Alternating Gradient Synchrotron (AGS) at Brookhaven National Laboratory in Upton, NY, and two with the Heavy Ion Medical Accelerator (HIMAC) at the National Institute of Radiological Sciences in Chiba, Japan. The features of the six experiments are summarized in Table 2. For each experiment, the beam energy exiting the accelerator and passing through the beam transport system was accurately known since only ions with the correct rigidity will survive transport to the experimental area. We performed calculations using a careful numerical integration of the Bethe-Bloch equation to determine energy loss in all components upstream of the TEPC gas volume, including vacuum windows and detectors. In this way we were able to determine the precise energy of the ^{56}Fe particles incident upon the TEPC. Additional screening of energy was done in the off-line analysis by using dE/dx in silicon detectors located immediately upstream and downstream of the TEPC to select only ^{56}Fe particles. During the experiment BNL97_2, 8.2-cm of polyethylene was placed in the particle beam upstream of all experimental apparatus to reduce the energy of the primary beam. During the BNL98 experiment, this procedure was repeated with 12.5 cm of polyethylene in the beam.

The same spherical TEPC (Far West Technologies, Inc., Goleta, CA) was used in all six experiments. The TEPC had an active volume 12.7 mm in diameter and a tissue-equivalent wall 2.54 mm thick. The active volume was filled with a propane-based tissue-equivalent gas at a pressure of 33 Torr, simulating a sphere of tissue having a diameter of 1 μm. Calibration was accomplished using an internally mounted ^{244}Cm α-particle source that was mounted with a gravity-controlled gate. When the TEPC was inverted from its operational orientation, the gate opened and α particles emanating from the source deposited 84.15 keV in the TEPC

gas cavity. Calibrations were also performed using maximum energy deposition from recoil protons generated in the wall using fast neutrons from a plutonium-beryllium source. The two methods agreed to within 2%.

In each of the six experiments, the energy signal from the TEPC was sent to an EG&G ORTEC (Oak Ridge, TN) charge-sensitive preamplifier, the output of which went to two separate EG&G ORTEC shaping amplifiers. The gains of the two shaping amplifiers were set so that the difference in amplification was approximately a factor of 12. These signals were sent to an analog-to-digital converter (ADC) dedicated to each amplifier.
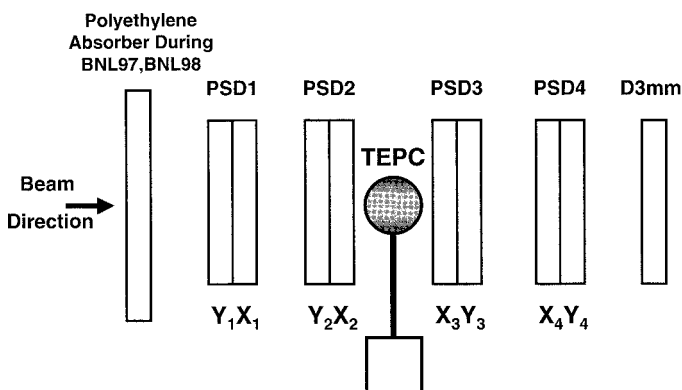
The TEPC was positioned within a particle spectrometer (Fig. 1) that measured individual particle events during the experiment. Four pairs of position-sensitive detectors (PSDs; denoted PSD1–PSD4 in Fig. 1) were used to track both the position and the energy of each particle as it passed through the apparatus. An individual PSD measured a single Cartesian coordinate (X or Y). Thus each pair determined the position of each particle in the transverse plane. The PSDs were lithium-drifted silicon detectors fabricated in the shape of circular disks, with radii of 20 mm and thickness between 800 μm and 1050 μm. The total charge collected, Q, on one side of the detector was proportional to the total amount of energy deposited in the PSD by the particle. On the other side of the detector, charge was divided between the top (q_1) and bottom (q_2) of a PSD (for the Y coordinate), or left (q_1) and right (q_2) of a PSD (for the X coordinate PSD). The amounts of charge collected in q_1 and q_2 can be related to the X or Y position of the incident particle (19). One X and one Y PSD were used in each PSD pair as seen in Fig. 1. One 3-mm-thick lithium-drifted silicon detector was placed downstream of the PSDs to provide additional information on energy deposition for each particle. Each of the PSD signals was sent to a dedicated ADC.

The data acquisition system was triggered by a coincidence between the TEPC signal and one of the PSD signals upstream of the TEPC. Iron ions can fragment into lighter ions as they pass through materials. The trigger threshold in the PSD was set so that only primary beam ions and fragments within a few charge units of the primary fired the trigger. Data were recorded on an event-by-event basis.

The data analysis system processed one and only one trigger at a time. The shaping time of the amplifiers is a few microseconds, and this is what is recorded by the ADCs. The system is gated off until all ADCs in the system are read and reset to zero. When this is completed, the system is enabled for the next trigger.

For each experiment, data for a minimum of 2 million triggers were recorded and stored on disk for subsequent analysis. The PSD detectors had an area slightly larger than the diameter of the TEPC. This meant that an incident particle could trigger the data acquisition system without passing through the TEPC. These events could be identified during the subsequent off-line analysis described below.

Time of flight was not the principal method of particle identification for these experiments. Secondary particles originating from fragmentation of the incident particle have velocities very similar to that of the original particle. Thus time of flight alone would not have sufficient resolution to identify secondary fragments.

FIG. 1. Diagram of the experimental arrangement, showing the position of the TEPC within the particle spectrometer.

DATA ANALYSIS

After the data acquisition was completed, information stored on disk was processed such that each event could be interrogated individually. The magnitude of the total charge, Q, from each PSD was proportional to the amount of energy deposited in the PSD by the traversing particle. The energy deposition spectrum for each PSD had a prominent peak corresponding to the primary ^{56}Fe particles and distinct peaks corresponding to particles with charges less than that of the primary particles. Because projectile fragments in the forward direction have velocities close to that of the incident beam, the energy deposition is approximately proportional to the square of the fragment charge. This information was used to select events where the incident ^{56}Fe particles passed through and did not fragment in the TEPC. A similar procedure was used for the beams degraded with a polyethylene absorber. It was a simple matter to select incident ^{56}Fe ions that slowed down but did not fragment in the degrader.

The two signals q_1 and q_2 produced by each PSD were related to either the X or the Y coordinate of the traversing particle. In certain regions of the PSDs, positions as calculated by the nominal method (19) are systematically in error; the errors are smallest near the center of the detectors and increase toward the edges. A calibration procedure was used to correct for these distortions, yielding improved accuracy in the position determination. A mask was fabricated, consisting of a thick (2.54 cm) brass plate with holes 0.8 mm in diameter drilled through it. The holes were spaced 6 mm apart in a radial pattern. During the experiments, dedicated data-taking runs were performed with the mask aligned with a PSD pair. The brass plate was thick enough to stop iron particles, so that only particles passing through the holes were registered in the PSD. Nuclear fragments produced in the brass could also emerge from the mask. These events were removed from the analysis because energy deposited in the downstream PSD did not correspond to unscattered ^{56}Fe particles passing through the holes. This procedure was repeated for each PSD pair. The data were used to obtain a transformation from q_1 and q_2 into the corresponding position. This alignment was achieved by performing univariate multiple regressions on the PSD response data, similar to the method described by Wong *et al.* (19) and Chapman (20).

In the data analysis, the X, Y and Z positions of a particle were defined relative to the center of the active volume of the TEPC, using information from PSD2. The Z axis is defined to be the primary beam direction; X and Y represented orthogonal coordinates in the transverse plane. The impact parameter is defined as the radial distance in millimeters from the center of the TEPC, so that particles traversing the full diameter of the active volume of the TEPC had impact parameters near 0 mm. Particles that traversed the TEPC at the interface between the active volume and wall had impact parameters equal to 6.35 mm. Particle
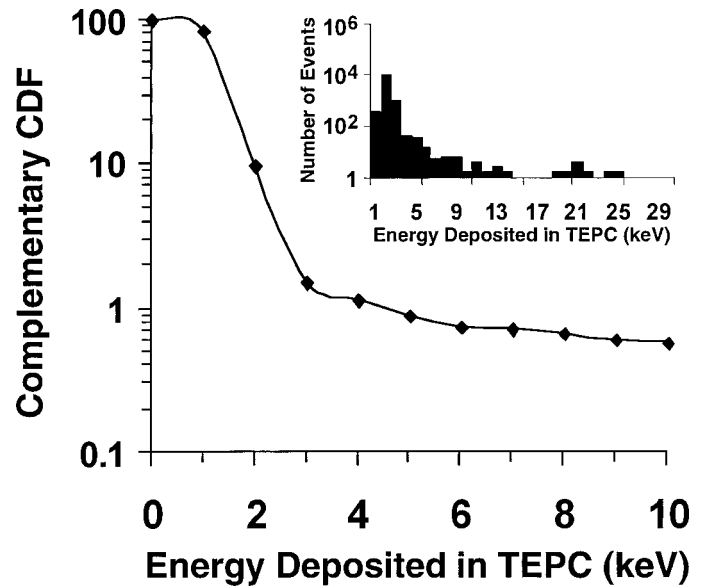

FIG. 2. Complementary cumulative distribution function (CDF) of energy deposition in the TEPC by 200 MeV/nucleon iron particles with impact parameters greater than 8.9 mm. The density distribution of the same events is shown in the inset.

events that grazed the outside edge of the wall had impact parameters equal to 8.89 mm.

Electronic Noise

There was no attempt to actively suppress electronic noise in the TEPC and amplifiers. During each run, random triggers were supplied to the data acquisition system. These events were easily recognized in the analysis as having an energy signal from the TEPC but with no energy deposited in the PSDs. The distribution of the TEPC signals on these events indicated that energy depositions below 3 keV cannot be distinguished from noise.

Many events that satisfied the iron-particle selection criteria in the PSDs had energy depositions below 3 keV in the TEPC. Virtually all of these events had impact parameters greater than 8.9 mm, which meant that they missed the TEPC altogether. Figure 2 shows the energy deposition distribution for these events. The primary graph in Fig. 2 is the complementary cumulative distribution of events when the impact parameter was greater than 8.9 mm. The inset in Fig. 2 is a histogram (i.e. density distribution) of the number of these same events as a function of energy deposition in the TEPC. This figure illustrates that there are occasional high-energy deposition events that occur at impact parameters greater than 8.9 mm. A comparison of the data found in Fig. 2 and the distribution of random-trigger events concluded that these two spectra were virtually identical. In both spectra, 99% of the events had energy depositions of less than 3 keV.

A scatter plot of energy deposition in the TEPC as a function of impact parameter for impact parameters greater than or equal to 8.9 mm is shown in Fig. 3. A χ^2 test of
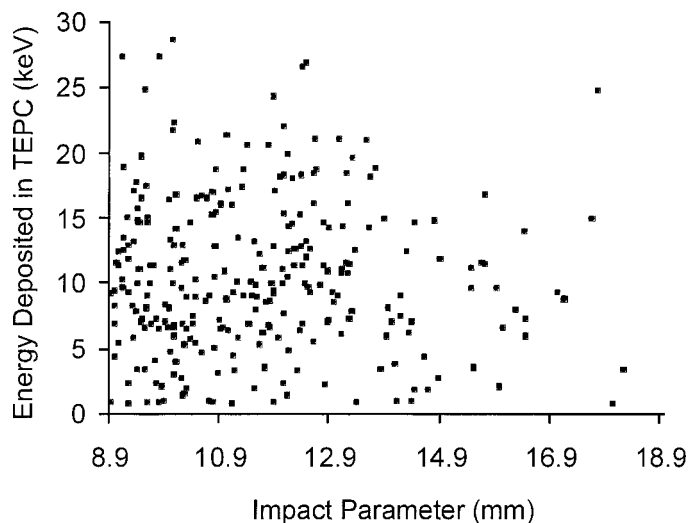
FIG. 3. Scatter plot of energy deposition in the TEPC as a function of impact parameter for 200 MeV/nucleon iron particles with impact parameters greater than 8.9 mm.

independence was performed on the events shown in Fig. 3. The χ^2 test was constructed to determine if there was a correlation between the energy deposited in the TEPC and the impact parameter of the event. The results of this test concluded that there was no statistical basis for any correlation between the energy deposited in the TEPC and the impact parameter of these events ($P = 0.62$). A χ^2 test of independence performed on events from the same experiment with impact parameters less than 8.9 mm showed that there was a strong dependence between energy deposited and impact parameter ($P = 1 \times 10^{-87}$). We conclude that the energy deposition in the TEPC by particle events with impact parameters greater than 8.9 mm were consistent

with electronic noise. These events were therefore excluded from further analysis.

Formation of Uniform Incident Fluence

The fluence of iron ions through the TEPC was not spatially uniform. To obtain the complete response of the TEPC for a uniform beam, the data for all incident iron particles were separated into a grid with a resolution of 1 mm $\times$ 1 mm. The corresponding event-size distributions for each grid were normalized to one incident particle and the spectra for each grid combined to form the response for uniformly incident iron ions. This distribution is referred to as the response function for the spherical TEPC. The response function for a given experiment was used to obtain average values corresponding to absorbed dose, D, frequency-averaged lineal energy, $\bar{y}_F$, and dose averaged lineal energy, $\bar{y}_D$.

Track Structure Model Calculations

A radial track structure model developed by Cucinotta *et al.* (*21*) was used to compute energy depositions in spherical volumes for comparison with the measured data. The output of this model was in the form of dose in water (Gy) at discrete radial distances from an HZE particle track. An example of the predictions of this model for ^{56}Fe at 360 MeV/nucleon is shown in Fig. 4. The model does illustrate that a large majority of the energy deposition occurs from very low-energy electrons produced near the center of the track.

These dose distributions were then superimposed on a sphere simulating incident ^{56}Fe particles at different impact parameters. Integrating the dose as a function of volume and using the appropriate density yielded energy deposi-
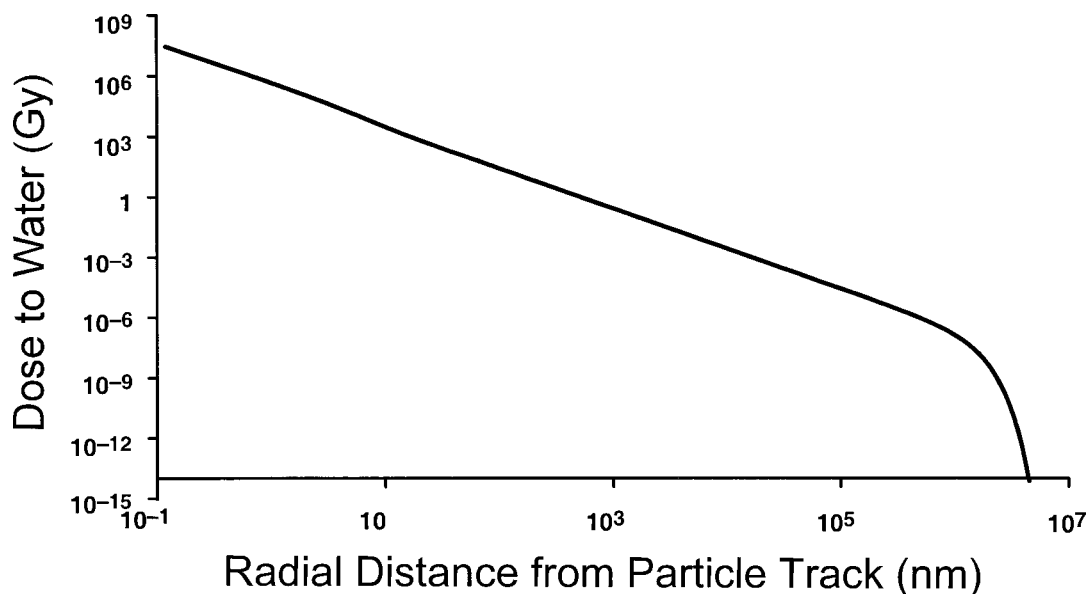

FIG. 4. The radial dose distribution from a 360 MeV/nucleon ^{56}Fe-particle track in water as calculated by the radial dose model (*21*).
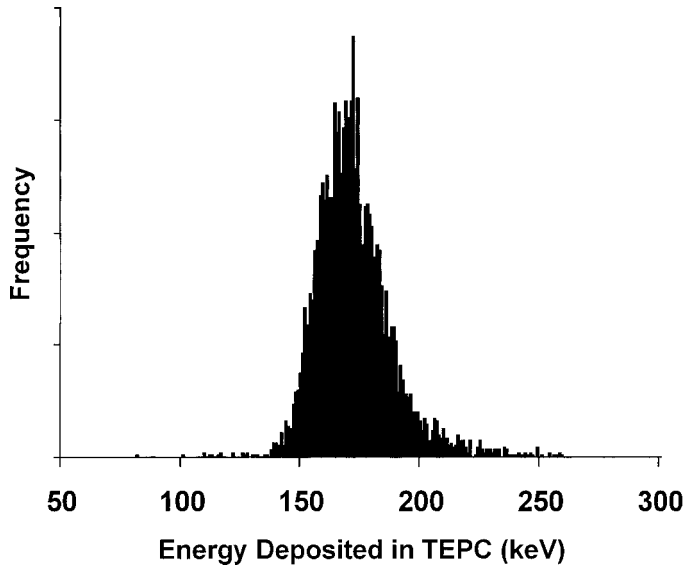
FIG. 5. Distribution of energy deposited in the TEPC by 360 MeV/ nucleon iron particles passing through the center of the detector with impact parameters less than 0.5 mm.

tion. Any energy deposited by the track for radii outside of the sphere was considered to have escaped the sensitive volume and was therefore not recorded. This provided an estimate of the reduction of LET due to δ rays escaping the volume of interest. The calculation was first performed assuming that the ^{56}Fe particle was passing through a homogeneous medium. In a second calculation, a heterogeneous medium was simulated to take into account the wall of the spherical TEPC, which has a density approximately 14,000 times greater than the gas cavity. Thus it was possible to estimate the influence of δ rays entering the gas cavity from ionization of atoms in the high-density wall. This computation simulated only the radial extension of the track and did not take into account any forward transport of electrons as the ^{56}Fe particle passed through the high-density wall before entering the sensitive volume of the detector.

RESULTS

Figure 5 shows the distribution of energy deposited in the TEPC by 360 MeV/nucleon ^{56}Fe particles with impact
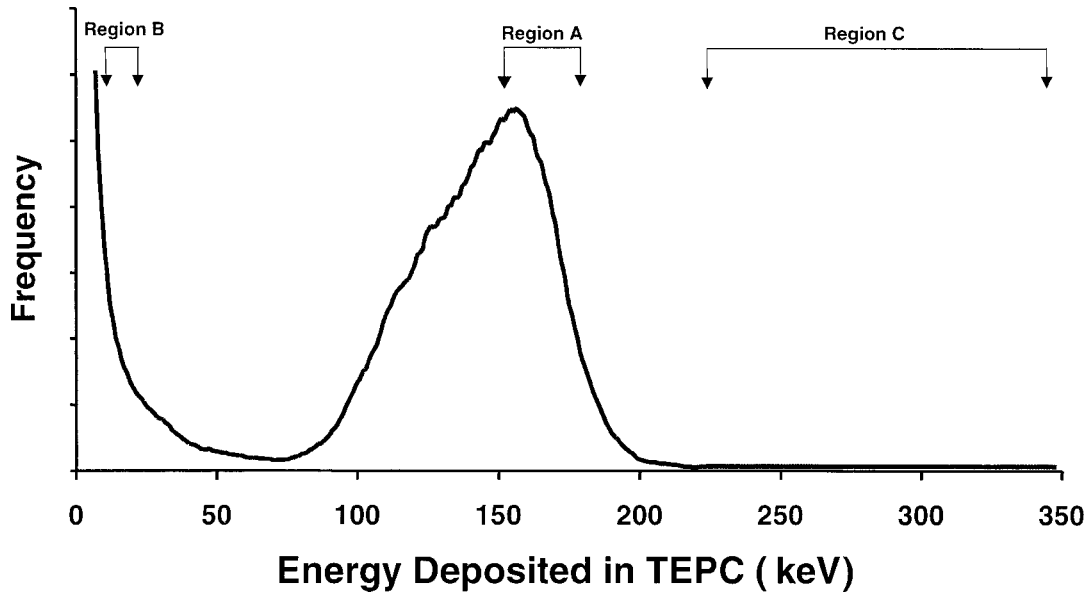
parameters of less than 0.5 mm, i.e., particles passing through the center of the detector. The path length of particles through the active volume of the TEPC changes by less than 2% as the impact parameter of the particle goes from 0 mm to 1 mm. Since the estimated uncertainty in the position measurement of the particles was less than 0.5 mm, the particle path lengths through the detector for events in this distribution were therefore known to within a 2% uncertainty. The mean of the distribution is 173 keV (FWHM 16%). The variance in the energy deposition in the main peak of this distribution is almost entirely attributable to variations due to energy-loss straggling and gas multiplication within the TEPC. The LET of a 360 MeV/nucleon ^{56}Fe ion is 214 keV/μm, so that on average only 81% of the energy transferred to the gas in the sensitive volume is actually deposited in the volume. Similar results were observed for all incident energies and are summarized in Table 3.

Figure 6 shows the complete response of the spherical TEPC for a uniformly incident beam of 360 MeV/nucleon iron particles. There is a broad distribution of energy depositions, with a peak near 160 keV and a large number of events with very small energy depositions, continuing below 50 keV. As described earlier, these are significantly above the electronic noise (99% of which is below 3 keV), and the number of events does not correspond to the expected chord length distribution for a uniformly incident beam of particles incident upon a sphere (i.e. μ-randomness). There is also a long tail of events with very large energy depositions, above 200 keV. Some of these events deposit more than twice the energy expected for a particle with this LET having the maximum trajectory through the sphere. Data from the other experiments showed that the shape of the response functions were similar for all energies.

To understand the shape of the response function, the energy deposition distribution was separated into three regions, A, B and C, as shown in Fig. 6. The X and Y coordinates of the incident particles in each region were plotted in a two-dimensional histogram with the base of the histogram corresponding to the X-Y coordinate when $Z = 0$ (i.e. center of the sphere in the direction of the beam). The results for all three regions are shown in Fig. 7.

TABLE 3
Summary of Data and Model Calculations for ^{56}Fe Particles

^{56}Fe-particle beam energies (MeV/nucleon)	LET of ^{56}Fe particles (keV/μm)	Energy deposited for events with impact parameter = 0 mm (keV)		(keV/μm)		
		Data mean (FWHM)	Model Mean	$\bar{y}_F$	$\bar{y}_D$	Λ
200	302	254 (35)	148	199	328	309
360	214	173 (28)	101	146	216	227
540	179	136 (24)	83	134	173	178
700	163	127 (19)	74	125	159	N/A
790	157	117 (13)	71	118	153	N/A
1000	149	116 (12)	65	106	147	154

FIG. 6. Probability density distribution (i.e. response function) of energy deposited in the TEPC by a uniform beam of iron particles at 360 MeV/nucleon. Three regions of energy deposition are indicated as A, B and C.

Events in region A are due to ions that pass through the center of the detector. Events in the broad peak from 50 to 200 keV correspond to particles passing through the sensitive volume of the TEPC (not shown). The small energy depositions in region B are from particles that pass through an annular area corresponding to the dimensions of the plastic wall of the TEPC. Electrons that originate in the wall and manage to penetrate into the sensitive volume cause these events. The very large energy depositions in region C also have an annular pattern, as well as a cluster of events along a line through the detector. The events in this annulus have a mean impact parameter that is very near the diameter of the sensitive volume. Thus when an iron ion grazes the inside edge of the wall, a large number of soft δ rays penetrate into the sensitive volume and create a large pulse that resembles the passage of a very high-LET particle through the gas volume. The events along the centerline are generated when the iron particle passes through the sensitive volume and strikes the anode or grid wires. These wires are very thin (45 μm) with high density ($\rho = 7.8$ g cm^{-3}). The resulting burst of electrons from the wire produces a large pulse comparable to that generated by the passage of a very high-LET particle.

Energy deposition as a function of impact parameter was calculated for each ^{56}Fe-particle beam energy. Figure 8 shows the results for 360 MeV/nucleon. This is not weighted by the fluence of particles at each impact parameter but should interpreted as the average energy deposited per incident particle having a given impact parameter. The solid black line represents energy deposition given by LET $\times$ chord length, where the chord length is a simple geometric function of impact parameter. For this case, energy deposition is maximum when the particle passes through the center of the sphere, and goes to zero when the impact

parameter is equal to the radius of the sphere. The black circles are obtained from the data and correspond to the mean energy deposited for the trajectory associated with the given impact parameter. The combined uncertainty in the estimated impact parameter and mean energy deposition is of the order of the symbol size. The procedure for determining the mean energy deposited was similar to that used by Rademacher *et al.* (*18*). For impact parameters near zero, the data show an average energy deposition that is about 20% less than this simple LET approximation. As the impact parameter increases, the data show that energy deposition becomes greater than the LET approximation and has a narrow peak of very large energy deposition just as the particle passes through the inside edge of the wall. Similar results were observed by Rademacher *et al.* for 1050 MeV/nucleon iron particles (*18*). This peak is the result of numerous soft electrons produced in the wall with sufficient energy to enter the cavity at grazing incidence.

The dashed gray line in Fig. 8 shows a calculation of energy deposition in a homogeneous medium obtained by spatially integrating the radial track model of Cucinotta *et al.* (*21*). The model predicts that for zero impact parameter, more than 50% of the energy transferred by the ^{56}Fe ion escapes the 1-μm-diameter sphere, in strong contrast to the data, which show about 20% losses. This difference is attributed to δ rays generated in the front wall of the detector that enter the sensitive volume and contribute to the measured energy distribution. The radial dose model does not include this forward component of electrons. If this is the case, it follows that the enhancement of δ rays from the forward wall does not fully compensate for the δ rays that escape the sensitive volume. Thus, for these events, charged-particle equilibrium is not achieved.

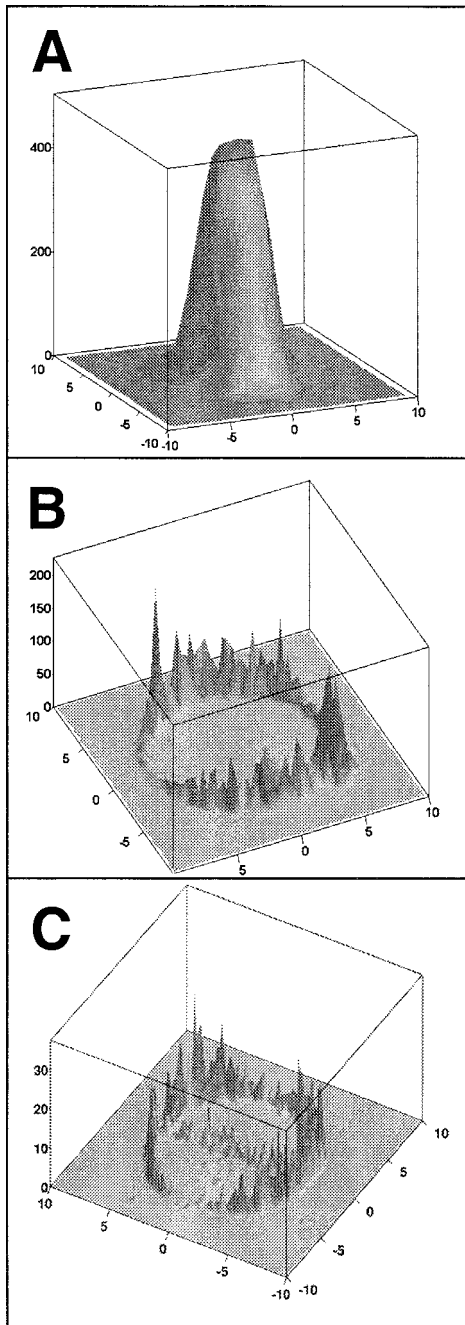The solid gray line in Fig. 8 represents energy deposition

FIG. 7. Three-dimensional histograms corresponding to the three regions of energy deposition indicated in Fig. 6. The X and Y coordinates represent the particle location in the plane normal to the beam axis. Z coordinates represent frequency of particle events.

FIG. 8. Mean energy deposited when a 360 MeV/nucleon ^{56}Fe particle has a specified impact parameter through the TEPC. The filled circles are the data. The thin black line was drawn through the circles is to guide the eye. The thick black line was obtained by multiplying the LET of 360 MeV/nucleon ^{56}Fe ions by the chord length through the detector volume at the given impact parameter. The dashed gray line was obtained from calculations using the radial dose model (*21*) assuming a homogeneous density surrounding the simulated spherical volume. The solid gray line was obtained from calculations using the radial dose model assuming heterogeneous density between the TEPC cavity and wall.

using the radial dose model for the heterogeneous geometry that takes into account the difference in density between the gas and the wall that surrounds the gas cavity. The spatial density of electrons generated in the wall is much higher than that of electrons generated in the gas, but the radial dimensions of the track are also reduced. The results of the model are similar to the homogeneous case for small impact parameters, but the heterogeneous model predicts an enhancement in energy deposition near the edge of the
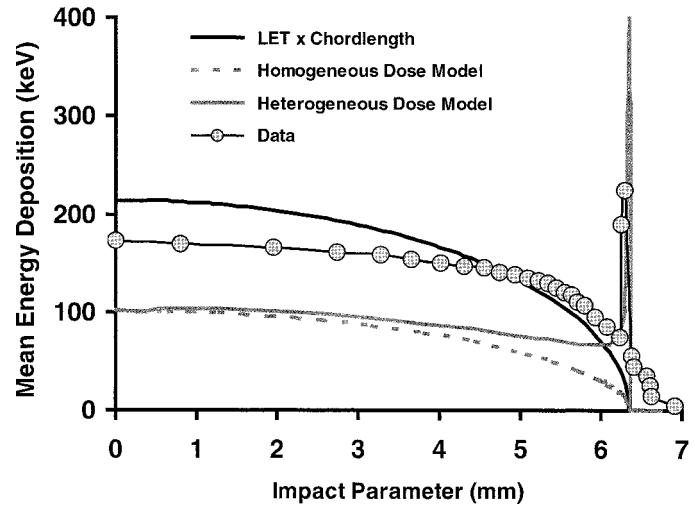
sensitive volume, similar to that seen in the data. This analysis was repeated for all energies, and the results are summarized in Table 3.

As shown above, charged-particle equilibrium was not achieved for iron particles passing through the center of the TEPC. The data were analyzed to determine if energy deposition integrated over the complete response function was sufficient to provide a correct estimate of absorbed dose. This analysis was performed by computing the LET, Λ, of a monoenergetic uniform fluence of particles, that would give the same dose as that recorded by integrating the response function to the TEPC. This calculation took into account the projected surface area of the complete detector (cavity plus wall) rather than just the cavity, since there were many recorded events from particles that missed the cavity but passed through the wall. If Λ was equal to LET, the TEPC provided an accurate estimate of absorbed dose. The results shown in Table 3 and Fig. 9 indicate that Λ was within 6% of the LET for the incident particle.

The energy deposition patterns in a TEPC are related to the LET of the incident heavy ions in a very complicated way. Using a TEPC to estimate quality factors has always been a desirable feature when applied to radiation protection dosimetry. To investigate this, the response functions were converted into distributions of lineal energy and used to determine frequency-averaged lineal energy, $\bar{y}_F$, and dose-averaged lineal energy, $\bar{y}_D$. The results are shown in Table 3 and Fig. 9. For the ideal case where energy deposition is LET $\times$ chord length, $\bar{y}_F$ should be identical to LET. It can be seen that for ^{56}Fe particles at these energies, mea-
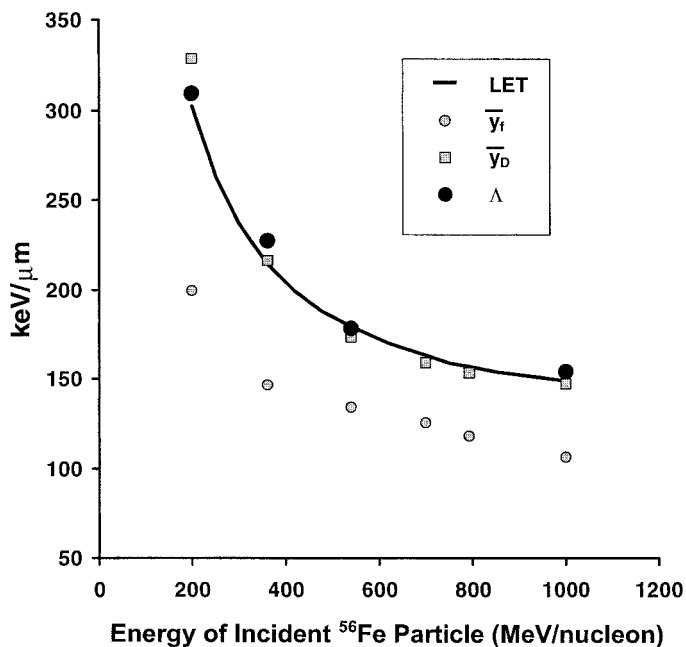
FIG. 9. The true value of LET for ^{56}Fe particles as a function of energy. Also shown are the frequency mean lineal energy, $\bar{y}_F$, dose mean lineal energy, $\bar{y}_D$, effective LET, Λ, obtained from the data at 200, 360, 540, 700, 790 and 1000 MeV/nucleon.

FIG. 10. Bar graphs showing estimates of quality factor as a function of energy for ^{56}Fe particles. The true quality factor, $Q(L)$, is obtained from the exact value of LET, at each energy. $Q(L = \bar{y}_D)$ is obtained using values of $\bar{y}_D$ from the data. $Q(L = y)$ is obtained from the data assuming that the measured distribution $f(y)$ is equivalent to the LET distribution of the incident particles.

sured values of $\bar{y}_F$ are consistently lower than LET due to the escape of electrons from the sensitive volume. However, $\bar{y}_D$ is always within 8% of LET.

We have computed quality factors using the known LET of the monoenergetic ^{56}Fe-particle beams and data from the TEPC. The true value of Q was obtained directly from ICRP Report 60 (*19*) using the LET of the incident monoenergetic beam. The quality factor was also computed using the assumption that the distribution of LET was identical to the measured distribution $f(y)$. For this case the dose as a function of y, $D(y)$, and $Q(L = y)$ from ICRP Report 60 were combined to form an estimate of Q. In another case, $Q(L = \bar{y}_D)$ was determined from only a single value of L assumed to be equal to $\bar{y}_D$ obtained from $f(y)$. These results are shown in Fig. 10. For monoenergetic beams, $Q(L = y)$ overestimated the true quality factor be as much as 20%, whereas $Q(\bar{y}_D)$ was always within 4% of the true quality factor. The same computation was performed assuming a uniform mixture of ^{56}Fe particles at each of the six energies. For this case, $Q(L = y)$ overestimated Q by 18% and $Q(\bar{y}_D)$ underestimated Q by 3%.

CONCLUSIONS

We have measured the response of a spherical tissue-equivalent proportional counter to ^{56}Fe-ion beams at several energies between 200 and 1000 MeV per nucleon. The experiments were performed at the AGS in Brookhaven National Laboratory in the U.S. and at the HIMAC at the National Institute for Radiological Sciences in Japan. Particles wer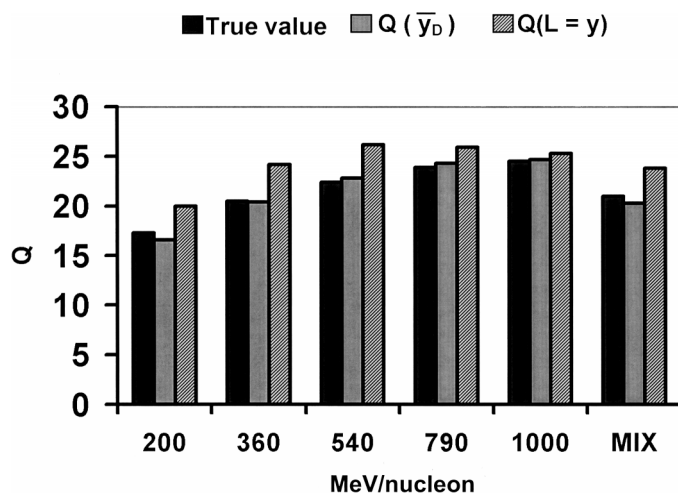e detected with a spectrometer that recorded the charge and position of each ion immediately upstream and downstream of the TEPC. Approximately 10^6 events were recorded for each experiment and analyzed off-line. The results reported here were for a uniform beam of iron particles that entered and exited the detector without any charge-changing nuclear interactions. In all cases, the gas pressure was regulated to simulate a sphere of tissue 1 μm in diameter.

The data at all energies indicated that track structure influences the pattern of energy deposition in the sensitive volume. For particles that pass through the center of the sphere, approximately 20% of the LET escapes the 1-μm-diameter volume. A model describing the radial distribution of the track indicated that over 50% of the LET should escape this volume. Differences between the data and model are attributed to δ rays produced in the front wall of the detector that have sufficient forward momentum to enter the gas cavity and contribute to energy deposition. However, this δ-ray enhancement from the forward wall is not sufficient to compensate for ionization lost from electrons that escaped as the iron particle passed through the sphere.

There is also a strong enhancement of events with very small energy depositions. These events originate from iron particles that do not cross the sensitive volume but pass through the side walls of the TEPC. Since the density of the wall is more than 10,000 times that of the gas cavity, there are many more electrons generated in the wall; however, only a few of them have sufficient range to penetrate into the sensitive volume to produce a measurable energy deposition. Because the projected area of the wall normal to the beam is large, these events occur frequently and make a significant contribution to the response of the TEPC. These could easily be misinterpreted as incident particles with low LET.

When the trajectory of the iron particle through the wall is very close to the inside boundary of the gas cavity, a large number of electrons enter the sensitive volume, producing a signal that resembles that produced by the passage of a high-LET particle through the detector. Some of these events produce more than twice the energy deposited when the primary incident particle passes directly through center of the sensitive volume.

One other class of events is generated when the incident iron particle strikes the anode or the grid wires of the TEPC. Since the high-density wires are very thin, many δ rays can escape into the gas and produce a large pulse.

In spite of the complicated response function, the detector does give a reasonably good estimate of absorbed dose. There seems to be sufficient enhancement of energy deposition from δ rays produced in the wall to compensate for high-energy δ rays that escape the spherical volume. Thus, while charged-particle equilibrium is not preserved on an event-by-event basis, it is preserved when the detector response is integrated over the complete response function that includes particles that do not pass through the sensitive volume.

In general it is assumed that a necessary condition for charged-particle equilibrium is the presence of material thickness equivalent to the maximum energy of the secondary electrons. This is clearly demonstrated using build-up caps with ionization chambers exposed to high-energy photon beams. However, photons above 1 MeV produce a fairly uniform energy distribution of electrons. For HZE particles having energies greater than 400 MeV/nucleon, the ranges of maximum energy electrons exceed the 2.5-mm wall thickness of the TEPC used here. But as was seen from the model in Fig. 4, high-energy electrons make only a very small contribution to the dose from HZE particles. Most of the energy along the track is deposited by large numbers of soft electrons having ranges substantially smaller than 1 mm. Although a thicker wall may be desirable to achieve complete charged-particle equilibrium, the data indicate that the 2.5-mm wall provides a satisfactory approximation for iron ions up to 1000 MeV per nucleon.

A spherical TEPC does not make a direct measurement of LET for ^{56}Fe particles at these energies, and therefore such a TEPC should not be considered as an LET spectrometer. In the ideal case, the frequency-averaged lineal energy, $\bar{y}_F$, should be numerically equivalent to LET, but these data show that $\bar{y}_F$ is always significantly less than LET. However, dose-averaged lineal energy, $\bar{y}_D$, does approximate LET. Computations of quality factor indicated that using the assumption that $\Phi(L)$ is identical to $f(y)$ yields a value that overestimates the true quality factor by 20%. The quality factor determined only from the dose-averaged lineal energy, $\bar{y}_D$, is always within 4% of the true value. It could be argued that since radiation risks are not always known with high precision, either method might be suitable for estimating dose equivalent. It will be necessary to collect data for other ions to confirm the hypothesis that

$\bar{y}_D$ provides a satisfactory approximation to LET for the purposes of determining the quality factors for HZE particles.

REFERENCES

1. NCRP, *Guidance on Radiation Received in Space Activities.* Report 98, National Council on Radiation Protection and Measurements, Bethesda, MD, 1989.

2. NCRP, *Radiation Protection Guidance for Activities in Low Earth Orbit.* Report 132, National Council on Radiation Protection and Measurements, Bethesda, MD, 2000.

3. G. D. Badhwar, The radiation environment in low-Earth orbit. *Radiat. Res.* **148** (Suppl.), S3–S10 (1997).

4. G. D. Badhwar, F. A. Cucinotta, L. A. Braby and A. Konradi, Measurements on the shuttle of the LET spectra of galactic cosmic radiation and comparison with the radiation transport model. *Radiat. Res.* **139**, 344–351 (1994).

5. G. D. Badhwar, A. Konradi, A. Hardy and L. A. Braby, Active dosimetric measurements on shuttle flights. *Nucl. Tracks Radiat. Meas.* **20**, 13–20 (1992).

6. A. S. Johnson, G. D. Badhwar, M. J. Golightly, A. C. Hardy, A. Konradi and T. Yang, *Spaceflight Radiation Health Program at the Lyndon B. Johnson Space Center.* NASA Technical Memorandum 104782, 1993.

7. G. D. Badhwar, A. Konradi, W. Atwell, M. J. Golightly, F. A. Cucinotta, J. W. Wilson, V. M. Petrov, I. V. Tchernykh, V. A. Shurshakov and A. P. Labakov, Measurements of the linear energy transfer spectra on the MIR orbital station and comparison with radiation transport models. *Radiat. Meas.* **26**, 147–158 (1996).

8. G. D. Badhwar, A. Konradi, L. A. Braby, W. Atwell and F. A. Cucinotta, Measurements of trapped protons and cosmic rays from recent shuttle flights. *Adv. Space. Res.* **14**, 67–72 (1994).

9. T. Doke, T. Hayashi and T. B. Borak, Comparisons of LET distributions measured in low-Earth orbit using tissue-equivalent proportional counters and the position sensitive silicon-detector telescope (RRMD-III). *Radiat. Res.* **156**, 310–316 (2001).

10. W. Glass and L. Braby, A wall-less detector for measuring energy deposition spectra. *Radiat. Res.* **39**, 230–240 (1969).

11. R. C. Rodgers, J. F. Dicello and W. Gross, The biophysical properties of 3.9-GeV nitrogen ions. *Radiat Res.* **54**, 12–23 (1973).

12. P. Kliauga, R. D. Colvett, L. J. Goodman and Y. M. Lam, Microdosimetry of 400 MeV/AMU ^{12}C and 450 MeV/AMU ^{40}Ar beams. In *Proceedings of the Sixth Symposium on Microdosimetry* (H. G. Ebert and J. Booz, Eds.), pp. 1173–1183. Harwood Academic, London, 1978.

13. G. Luxton and P. Fessenden, Microdosimetric measurements of pretherapeutic heavy ion beams. *Radiat. Res.* **79**, 256–272 (1979).

14. J. F. Dicello and M. Wasiolek, measured microdosimetric spectra of energetic ion beams of Fe, Ar, Ne and C: Limitations of LET distributions and quality factors in space research and radiation effects. *IEEE Trans. Nucl. Sci.* **38**, 1203–1209 (1991).

15. J. F. Dicello, H. I. Amols, M. Zaider and G. Tripard, A comparison

of microdosimetric measurements with spherical proportional coun-
ters and solid-state detectors. *Radiat. Res.* **82**, 441–453 (1980).

16. N. F. Metting, H. H. Rossi, L. A. Braby, P. J. Kliauga, J. Howard,
    M. Zaider, W. Schimmerling, M. Wong and M. Rapkin, Microdosim-
    etry near the trajectory of high-energy heavy ions. *Radiat. Res.* **116**,
    183–195 (1988).

17. A. Ito and R. M. Henkelman, Microdosimetry of the pion beam at
    TRIUMF. *Radiat. Res.* **82**, 413–429 (1980).

18. S. E. Rademacher, T. B. Borak, C. Zeitlin, L. Heilbronn and J. Miller,
    Wall effects observed in tissue-equivalent proportional counters from

1.05 GeV/nucleon iron-56 particles. *Radiat. Res.* **149**, 387–395
(1998).

19. M. Wong, W. Schimmerling, M. H. Phillips, B. A. Ludewigt, D. A.
    Landis, J. T. Walton and S. B. Curtis, The multiple coulomb scatter-
    ing of very heavy charged particles. *Med. Phys.* **17**, 163–171 (1990).

20. P. L. Chapman, Applied regression methods. In A*pplications of Prob-
    ability and Statistics in Health Physics* (T. Borak, Ed.). Medical Phys-
    ics Publishing, Madison, WI, 2000.

21. F. A. Cucinotta, R. Katz, J. W. Wilson and R. R. Dubey, *Heavy Ion
    Track-Structure Calculations for Radial Dose in Arbitrary Materials.*
    NASA Technical Paper 3497, 1995.